Modeling Blowdown of Pipelines Under Fire Attack

Haroun Mahgerefteh and Muhammad Umar Abbasi
Dept. of Chemical Engineering, University College London, London WC1E 7JE, U.K.

DOI 10.1002/aic.11270
Published online July 25, 2007 in Wiley InterScience (www.interscience.wiley.com).

The development of a mathematical model for simulating the blowdown of pressurized hydrocarbon conveying pipelines under fire attack is described. The model is based on the resolution of the conservation equations using the method of characteristics. It accounts for real fluid behavior, pipeline mechanical strength, as well as phase and flow dependent transient heat transfer effects, and frictional pressure losses. Failure is assumed to occur when any one of the simulated triaxial thermal and pressure stresses in the pipeline wall exceed its ultimate tensile strength. The application of the model to a hypothetical example involving localized fire attack on an isolated natural gas pipeline reveals that the pipeline fails because of large thermal stresses on the outer surface in addition to the internal pressure stresses. The efficacy of emergency depressurization using different diameter relief valves as a means of protecting the pipeline mechanical integrity during fire attack is also quantitatively investigated.
 AIChE J, 53: 2443–2450, 2007
Keywords: pressurized pipelines, safety, loss prevention, pressurized flow, numerical analysis

Introduction

In recent years, pipelines have gained significant popularity as a means of transporting large amounts of pressurized hydrocarbons across the globe. These provide extraordinary quantities of energy products to industry and consumers, literally fuelling economies and way of life. However, their increasing use coupled with operation under more extreme conditions, such as high pressures, to maximize throughput have inevitably resulted in a significant rise in their failure frequency. Such accidents have often resulted in large number of casualties, including fatalities and significant environmental damage.[1]

In the U.S. there are more than 2.3 million miles of natural gas and hazardous liquid pipelines. These run under homes, near schools, and offices. Since 1986 there have been 5700 pipeline accidents resulting in 325 deaths, 1500 injuries, and more than $850 m environmental damage. On average, there is one pipeline accident every day. According to the U.S. Office for Pipeline Safety[2] every year more than 6 million gallons of hazardous material are spilled through pipelines.

The Belgium pipeline rupture incident on July 30, 2004 resulting in 27 deaths and 120 injuries[3] has since changed the historical perception that such incidents are mainly confined to outside of the European Union (EU).

In the U.K., more than 28,000 km of pressurized pipelines pass through both rural and populated areas. Of these ~20,000 km transport high-pressure natural gas above 7 bar, 7000 km multicomponent liquids, such as gasoline, and over 1000 km carry ethylene. Hundreds of kilometers of additional pipelines are currently being added to the U.K. pipeline infrastructure.

By the end of 2007, to address the U.K.'s growing energy needs, the Government plans to import large amounts of liquefied natural gas using marine tankers. Once treated and converted to its natural state, the gas is to be distributed across the U.K., using pressurized pipelines. It is estimated that up to $7 billion worth of gas will be fed into the U.K.'s supply over the next 15 years through this route.

Correspondence concerning this article should be addressed to H. Mahgerefteh at h.mahgerefteh@ucl.ac.uk.

The earlier has given rise to major public concern leading to several civil lawsuits awaiting hearing in the High Court.

Indeed a recent EU commissioned study[4] recognizes pipelines as a "major-accident hazard." Despite this, a greater use of pipelines is being promoted within the EU, including the development of major European pipeline networks. In response to this, a new European Directive[5] expected to come into effect by 2008, will require the hazard assessment of all pressurized pipelines containing appreciable amounts of hazardous materials. In the U.S. the above is already enacted in the U.S. Pipeline Safety Act 2000.[2] The Act goes on to require integrity management procedures that will reduce such risks to acceptable levels.

A major credible hazard involving pressurized pipelines is loss of mechanical integrity because of thermal loading during fire attack. In such circumstances, the determination of the subsequent discharge rate following rupture is important since it dictates all the major consequences associated with pipeline failure, including fire, explosion, dispersion, and environmental pollution. All of these parameters are key features of the Safety Case prepared by the pipeline operators. Safety authorities on the other hand use such data as the basis for controlling the risks to populated areas.

Ironically, despite the fact that pipelines pose a significantly greater hazard as opposed to pressurized vessels, all of the studies reported in the literature concerning modeling the impact of fire loading have been exclusively confined to the latter.[6–8] This is partly due to the more complicated nature of the large number of interacting processes involved during unsteady state flow in a pressurized pipeline as opposed to those for a fluid confined in a fixed volume vessel.

In this article, we report the development of a numerical model based on the method of characteristics (MOC) for predicting the transient triaxial pressure and thermal stresses in pressurized pipelines during localized jet fire attack. Failure is assumed to occur when the sum of these stresses exceed the pipe wall material ultimate tensile strength (UTS).

An important part of the study examines the efficacy of emergency depressurization as a means of protecting the pipeline mechanical integrity during fire attack.

Theory

The following interacting processes are simulated for the modeling the failure of the pressurized pipeline during fire attack:

(i) heat transfer between the escaping fluid, pipe wall, and the surrounding ambient;

(ii) real fluid flow dynamics, including the discharge and depressurization rates;

(iii) transient pressure and thermal stresses within the pipeline wall.

Heat transfer within the pipe wall

A 2D finite difference method is employed for predicting the transient temperature profile within the pipe wall. In the case of conduction heat transfer, the governing differential equation for heat flow is given by Ozisik[9]

$$\kappa\left(\frac{\partial^2 T}{\partial x^2}+\frac{\partial^2 T}{\partial y^2}\right)=\rho c\frac{\partial T}{\partial \tau} \tag{1}$$

where k, the thermal conductivity (W/mK); c, specific heat capacity [J/(kg K)]; ρ, density (kg/m^3).

The earlier partial derivatives can be approximated by:

$$\frac{\partial^2 T}{\partial x^2}\approx\frac{1}{(\Delta x^2)}\left(T_{m+1,n}+T_{m-1,n}-2T_{m,n}\right) \tag{2}$$

$$\frac{\partial^2 T}{\partial y^2}\approx\frac{1}{(\Delta y^2)}\left(T_{m,n+1}+T_{m,n-1}-2T_{m,n}\right) \tag{3}$$

where Δx and Δy, respectively, represent the axial and vertical nodal distances, with the subscripts, m and n denoting the corresponding node locations.

The time derivative, $\frac{\partial T}{\partial \tau}$ in Eq. 1 may be approximated by

$$\frac{\partial T}{\partial \tau}\approx\frac{T^{p+1}_{m,n}-T^{p}_{m,n}}{\Delta\tau} \tag{4}$$

Combining Eqs. 2–4 and rearranging, yields

$$\frac{T^{p}_{m+1,n}+T^{p}_{m-1,n}-2T^{p}_{m,n}}{(\Delta x^2)}+\frac{T^{p}_{m,n+1}+T^{p}_{m,n-1}-2T^{p}_{m,n}}{(\Delta y^2)}=\frac{1}{\alpha}\frac{T^{p+1}_{m,n}+T^{p}_{m,n}}{\Delta\tau} \tag{5}$$

where $T^{p}_{m,n}$ and $T^{p+1}_{m,n}$, respectively, represent the nodal temperatures at the previous and the subsequent time steps, α is the thermal diffusivity.

For the convection boundaries (pipe wall/fluid/surrounding ambient), the nodal transient energy balance is made by setting the sum of energies conducted and convected into the node equal to the increase in internal energy. Following Holman[10] we have:

$$k\Delta y\frac{T^{p}_{m+1,n}+T^{p}_{m-1,n}}{\Delta x}+k\frac{\Delta x}{2}\frac{T^{p}_{m+1,n}+T^{p}_{m-1,n}}{\Delta y}+k\frac{\Delta x}{2}\frac{T^{p}_{m+1,n}+T^{p}_{m-1,n}}{\Delta y}+h\Delta y(T_\alpha-T^{p}_{m,n})=\rho c\frac{\Delta x}{2}\Delta y\frac{T^{p}_{m+1,n}+T^{p}_{m-1,n}}{\Delta\tau} \tag{6}$$

where h and T_α are the heat transfer coefficient and ambient temperature, respectively.

Figure 1 depicts the various heat transfer boundaries during depressurization or blowdown through a relief valve. These include:

(1) heat transfer between the outside ambient and the pipe wall, h_1;

(2) forced convective heat transfer between the escaping fluid and the discharge plane, h_2;

(3) forced convective heat transfer between the flowing fluid and the inner pipe wall, h_3.

The appropriate heat transfer coefficients are determined using standard correlations. In the case of the surrounding ambient and the pipewall heat transfer (h_1), a constant heat flux of 350 kW/m^2 (Ref. 11) is employed.

For fluid/pipeline wall heat transfer (h_3), we assume the flow during depressurization is fully developed turbulent. This is a reasonable assumption considering the relatively high Reynolds numbers ($>10^6$) during depressurization. Con-

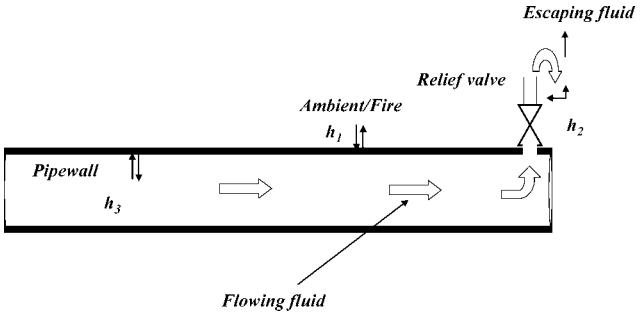

Figure 1. Schematic representation of the various heat transfer boundaries during depressurization under fire attack.

sequently, heat exchange between the discharging fluid and the pipe wall is due to forced, as opposed to natural convection. In the case of single-phase flow, the correlation proposed by Gnielinski[12] for flow in smooth pipes is used. For two-phase flow on the other hand, the correlation proposed by Steiner and Taborek[13] is employed. The mixture density, ρ_{mix} required for the calculation of the two-phase flow heat transfer coefficient is obtained from

$$\rho_{\text{mix}} = \frac{\rho_{\text{g}}\rho_1}{\rho_{\text{g}}(1-x)+\rho_1 x} \tag{7}$$

where ρ_1 and ρ_{g} are the gas and liquid densities, respectively, with x representing the fluid mass fraction.

Fluid dynamics

The governing theory for determining the fluid dynamics, such as the discharge rate and the fluid temperature, pressure, and velocity profiles along the pipeline following failure have been described in our earlier publications.[14–18] Briefly, the procedure involves the numerical solution of the mass, energy, and momentum conservation equations assuming 1D flow, using a suitable technique such as the MOC.[19]

The conservation equations for 1D flow in a pipeline expressed in terms of pressure (P), specific enthalpy (h_{e}), and flow velocity (u) as dependent variables are given by Oke et al.[20]:

$$[\rho T+\psi]\frac{dP}{dt} - \rho\psi\frac{dh_{\text{e}}}{dt} + \rho^2 a^2 T\frac{\partial u}{\partial x} = 0 \tag{8}$$

$$\rho\frac{du}{dt} = -\frac{\partial P}{\partial x} - \rho g\sin\theta + \beta_x \tag{9}$$

$$\rho\frac{dh_{\text{e}}}{dt} - \frac{dP}{dt} = q_{\text{h}} - u\beta_x \tag{10}$$

where θ, pipeline elevation (°); g, gravitational constant (m^2/s); s, specific entropy [kJ/(kg°C)]; a, speed of sound (m/s); q_{h}, net rate of heat flow from external sources to the fluid (kW/m^2); β_x, frictional force term; $\psi = \left(\frac{\partial P}{\partial s}\right)_\rho$.

The earlier outflow model, validated against field data[18] accounts for real fluid behavior as well as heat transfer and frictional effects. It is applicable to both isolated and unisolated flows where pumping at the high-pressure end continues despite puncture. Liquid and vapor phases are assumed to be at thermodynamic and phase equilibrium with one another traveling at the same velocity. This assumption is found to be generally valid in the case of rupture of long pipelines.[21,22]

The fluid approaching the release plane during depressurization can be either single or two-phase. If the backpressure is sufficiently low, the fluid accelerates through the relief valve at its maximum velocity and expands rapidly from the upstream to the orifice pressure. Consequently, condensation may occur, which results in two-phase flow. The procedure for determination of the discharge rate and the state of fluid phase at the release plane is described elsewhere.[23,24] In essence, it is based on carrying out an energy balance across the orifice assuming isentropic expansion coupled with thermodynamic and phase equilibrium.

The flow dependent wall friction force term is obtained using the Moody approximation to the Colebrook equation.[25]

Peng–Robinson equation of state[26] is used for obtaining the appropriate thermodynamic and phase equilibrium data. This equation has been shown to be particularly applicable to high-pressure hydrocarbon mixtures.[27,28] The number and the appropriate fluid phase(s) present at any given temperature and pressure on the other hand are determined using the stability test based on the Gibbs tangent plane criterion developed by Michelsen.[29–31] For unstable systems, the same technique also provides the composition of a new phase, which can be split off to decrease the Gibbs energy of the mixture. Pseudo-fluid properties for mixtures are calculated from the pure liquid and gas properties obtained from the EoS.

The speed of sound for real multicomponent single-phase fluids is obtained using standard expressions.[32] In the absence of an analytical solution, the speed of sound for two-phase mixtures is calculated numerically.[16]

Thermal and pressure stresses

The tangential, radial, and longitudinal thermal and pressure stresses used are those for thick-walled cylinders undergoing elastic deformation following nonuniform heating. The plastic deformation region is ignored because of the complications association with modeling such behavior.

Based on the normal stress failure criterion, failure is assumed to occur when either or both of the earlier total stresses exceed the vessel material's UTS.[33]

The 3D thermal stresses in the pipeline are obtained from the radial temperature profile $T(r)$ using the following equations[34]:

$$\sigma_t^T = \frac{M_1}{r^2}\left[\frac{r^2+a^2}{b^2-a^2}\int_a^b T(r)rdr + \int_a^r T(r)rdr - T(r)r^2dr\right] \tag{11}$$

$$\sigma_r^T = \frac{M_1}{r^2}\left[\frac{r^2-a^2}{b^2-a^2}\int_a^b T(r)rdr - \int_a^r T(r)rdr\right] \tag{12}$$

$$\sigma_l^T = M_1\left[\frac{2}{b^2-a^2}\int_a^b T(r)rdr - T(r)dr\right] \tag{13}$$

Table 1. Pipeline Conditions—Inventory (mol %): CH_4 (90.0) and C_3H_8 (10.0)

Feed pressure, bara	117
Feed temperature, K	293.15
Pipeline thickness, mm	19
Pipeline inner diameter, m	0.419
Pipeline density, kg/m^3	7854
Pipeline thermal conductivity, W/mK	53.6
Ambient temperature, K	293
Flame temperature, K	1500
Pipe roughness, mm	0.05

where $M_1 = \frac{\tau E}{1-\mu}$ with σ_t^T, σ_l^T, and σ_r^T, respectively, representing the tangential, longitudinal, and radial thermal stresses. a, pipe internal radius; b, pipe external radius; τ, coefficient of thermal expansion; E, modulus of elasticity; μ, Poisson's ratio.

The corresponding pressure stresses in the pipeline are obtained using the equations given by Popov[33] for thick-walled cylinders:

$$\sigma_t^P = \frac{Pa^2}{b^2 - a^2}\left(1 + \frac{b^2}{r^2}\right) \tag{14}$$

$$\sigma_r^P = \frac{Pa^2}{b^2 - a^2}\left(1 - \frac{b^2}{r^2}\right) \tag{15}$$

$$\sigma_l^P = \frac{Pa^2}{b^2 - a^2} \tag{16}$$

The total resident stresses at any location within the pipeline wall are determined from the sum of the thermal (Eqs. 11–13) and pressure stresses (Eqs. 14–16).

Results and Discussion

The following represents the results of the application of earlier model to a hypothetical example involving a carbon steel pipeline containing pressurized natural gas under localized jet fire attack. Table 1 shows the pipeline characteristics and the prevailing conditions.

For simplicity, the pipeline thermal conductivity is assumed to be independent of temperature. In practice, the thermal conductivity for carbon steel is reduced by about 20% over the temperature range 20–400°C. A reduction in the thermal conductivity with temperature increases the temperature gradient across the pipe wall thereby increasing the thermal stresses hence leading to earlier pipeline failure times. This effect is counteracted by a reduction in the integral pipe wall temperature (see Eq. 17), which will increase the pipe wall UTS and hence delay pipeline failure. The net result will depend on the balance between these two counteracting effects, the outcome of which will depend on a detailed analysis of the particular system under study.

For the sake of an example, it is assumed that a 10-m section of the uninsulated carbon steel pressurized pipeline is completely enveloped by a jet fire a distance of 390 m from one of its ends.

Two types of failure scenarios are simulated. The first deals with the impact of direct jet fire impingent on the intact pipeline. For reference purposes, this is referred to as "isolated pipeline failure." In the second case, hereby referred to "unisolated pipeline failure," the effect of emergency depressurization using various diameter relief valves on the pipeline mechanical integrity during fire attack is simulated.

Isolated pipeline

In the case of isolated pipeline, it is assumed that prior to jet fire attack, the pipeline pressure and temperature are constant throughout its entire length.

Figure 2 shows the variation of the outer (curve A) and inner wall (curve B) temperatures as a function of time for the 10-m section of the pipeline under jet fire attack. As it may be observed, the outer wall temperature exposed to fire reaches a maximum temperature 540 K some 300 s following thermal loading. Given the inner wall temperature of 290 K, the corresponding temperature gradient across the pipewall is about 250 K. A comparison of the resulting thermal and pressure stresses with the pipeline UTS will dictate if and when the pipeline fails during fire attack. This will be demonstrated later.

Interestingly, the corresponding line pressure versus time data in the same time frame reveal that the thermal loading of the pipeline does not result in any appreciable change in the line pressure. This is because of the large heat capacity of the 1-km pipeline.

Figures 3–5 respectively show the corresponding time dependent variations of the total normalized radial, longitudinal, and tangential stresses across the pipe wall for the isolated pipeline section exposed to fire attack.

The various stress profiles have been normalized with respect to the pipeline material of construction's UTS data

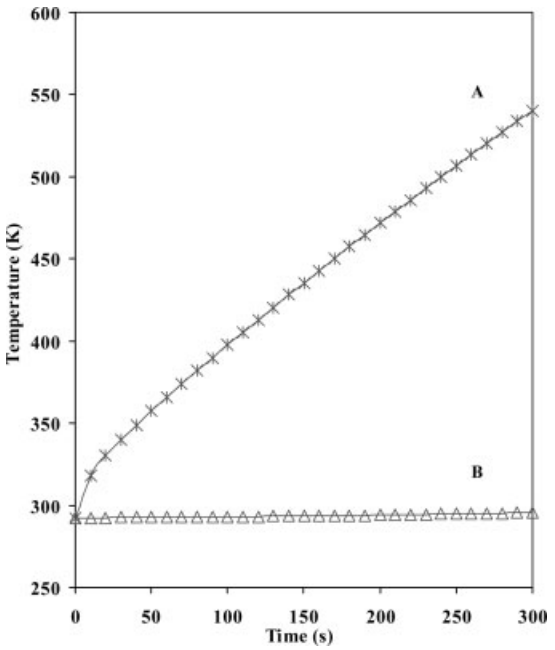

Figure 2. The variation of pipe wall temperature with time during jet fire attack for the isolated pipeline.

Curve A: outer wall; curve B: inner wall.

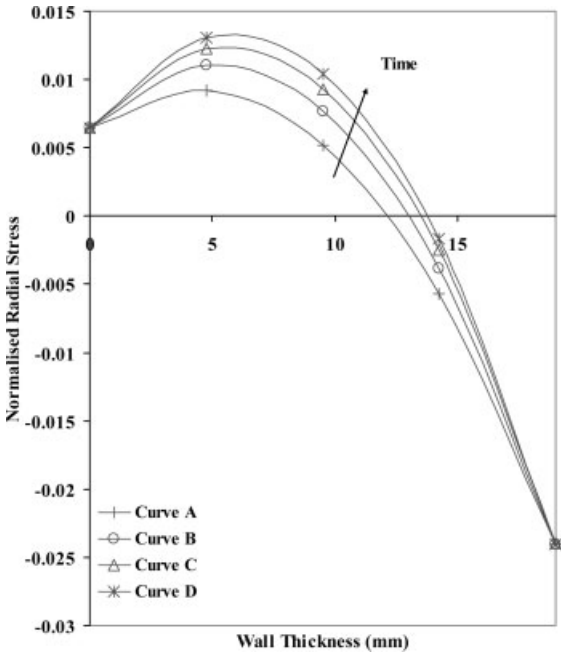

Figure 3. The variation of the normalized radial stress across the pipe wall at different time intervals for the isolated pipeline under fire attack.

Curve A: 50 s, $\Psi(K) = 325.07$; curve B: 100 s, $\Psi(K) = 345.33$; curve C: 150 s, $\Psi(K) = 364.48$; curve D: 200 s, $\Psi(K) = 382.89$.

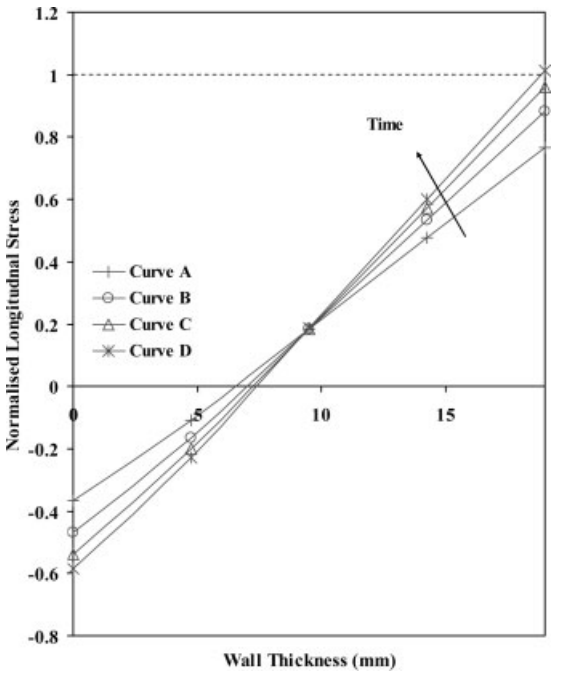

Figure 4. The variation of the normalized longitudinal stress across the pipe wall at different time intervals for the isolated pipeline under fire attack.

Curve A: 50 s, $\Psi(K) = 325.07$; curve B: 100 s, $\Psi(K) = 345.33$; curve C: 150 s, $\Psi(K) = 364.48$; curve D: 200 s, $\Psi(K) = 382.89$.

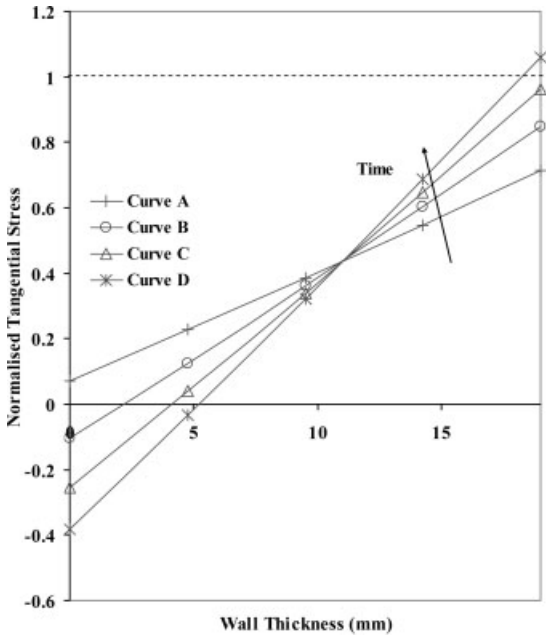

Figure 5. The variation of the normalized tangential stress across the pipe wall at different time intervals for the isolated pipeline under fire attack.

Curve A: 50 s, $\Psi(K) = 325.07$; curve B: 100 s, $\Psi(K) = 345.33$; curve C: 150 s, $\Psi(K) = 364.48$; curve D: 200 s, $\Psi(K) = 382.89$.

for carbon steel[35] at the prevailing pipeline integral temperature, $\Psi(K)$. This is given by

$$\Psi(K) = \frac{\int_a^b T(r,t)\,dr}{b-a} \tag{17}$$

Normalized stress values equal or greater than unity indicate pipeline failure. Positive and negative values on the other hand represent tensile and compressive stresses, respectively.

Referring to Figure 3, it is clear that pipeline failure in the radial direction in the time domain under consideration (300 s) is impossible since the normalized stress values remain well below unity throughout.

Figures 4 and 5 on the other hand reveal much larger normalized longitudinal and tangential stresses. The relatively low normalized compressive stresses at the inner wall rapidly transform into tensile stresses toward the outer wall. Comparing the data given in Figures 4 and 5 it is clear that the pipeline fails in the tangential direction due to prevailing tensile stresses some 160 s following fire attack. This failure mechanism known as bulging is schematically represented in Figure 6.

Figure 7 shows the transient variations of the thermal (curve A, σ_T) and pressure stresses (curve B, σ_p) in the outer pipeline wall section during fire attack. Curves C and D on the other hand show the corresponding pipeline wall total stress ($\sigma_T + \sigma_p$) and UTS data. As it may be observed, the dominant failure mechanism for the pipeline is due to thermal stresses. These, in contrast to the pressure stresses, rapidly increase with time during fire loading. The pipeline fails

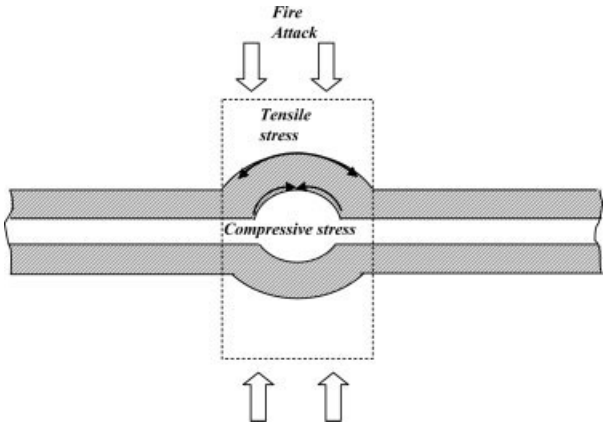

Figure 6. Schematic representation of bulging pipeline failure following fire attack.

at the intersection of curves C and D; 150 s following jet fire attack.

Unisolated pipeline failure

The effect of emergency depressurization on the resulting thermal and pressure stresses during fire attack is investigated in the following.

Figure 8 shows the variation of the line pressure as a function of time during emergency depressurization through different diameter relief valves [25 mm (curve A), 50 mm (curve B), 75 mm (curve C), and 100 mm (curve D)] under fire attack. The corresponding data for the isolated pipeline

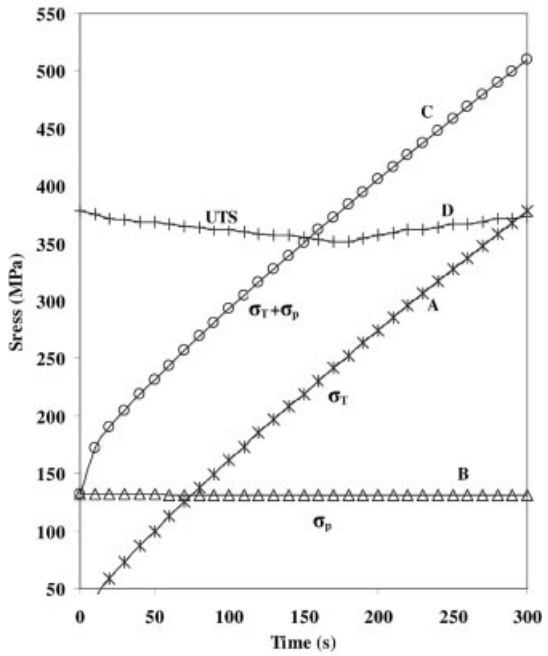

Figure 7. The variation of the various outer wall tangential stresses as a function of time for the isolated pipeline under fire attack.

Curve A: thermal stress, σ_T; curve B: pressure stress, σ_P; curve C: total stress, $\sigma_P + \sigma_T$; curve D: UTS.

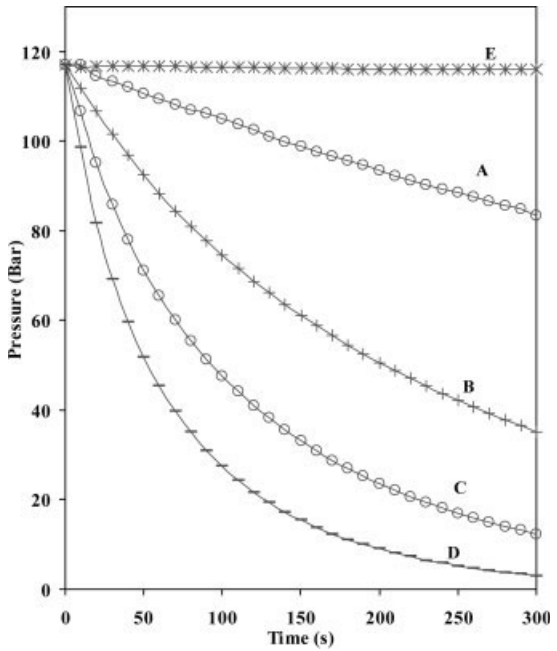

Figure 8. Variation of line pressure with time during depressurization using different diameter relief valves during fire attack.

Curve A: 25 mm; curve B: 50 mm; curve C: 75 mm; curve D: 100 mm; curve E: isolated pipeline.

are also given for comparison (curve E). A discharge coefficient of unity is assumed. As it may be observed from the data, the increase in the relief valve diameter has a significant impact on the pipeline depressurization rate and hence the resulting pressure stresses.

An investigation of the corresponding thermal and pressure stresses reveals that much the same as that for the isolated case, the pipeline failure mode during emergency depressurization under fire attack is due to tangential tensile stresses at the outer pipeline wall.

Figure 9 represents the variation of the total tangential stresses as a function of time during emergency depressurization using different relief valve diameters under fire attack. Curves A–D respectively show the total (pressure + thermal) outer wall stresses for 25, 50, 75, and 100 mm relief valve diameters. Curve E shows the corresponding data for the isolated intact pipeline (no pressure relief). Curve F on the other hand shows the time dependent variation of the UTS.

As it may be observed from the data, emergency depressurization has a significant impact on delaying the time for pipeline failure. The corresponding failure times for the isolated pipeline, 25, 50, 75, and 100 mm relief valve diameters are 150, 190, 210, and 220 s, respectively. It is noteworthy that despite delaying failure times, for the conditions tested, emergency depressurization does not circumvent pipeline failure.

Conclusion

The development of a mathematical model for simulating the loss in the mechanical integrity of pressurized pipelines under fire attack is presented.

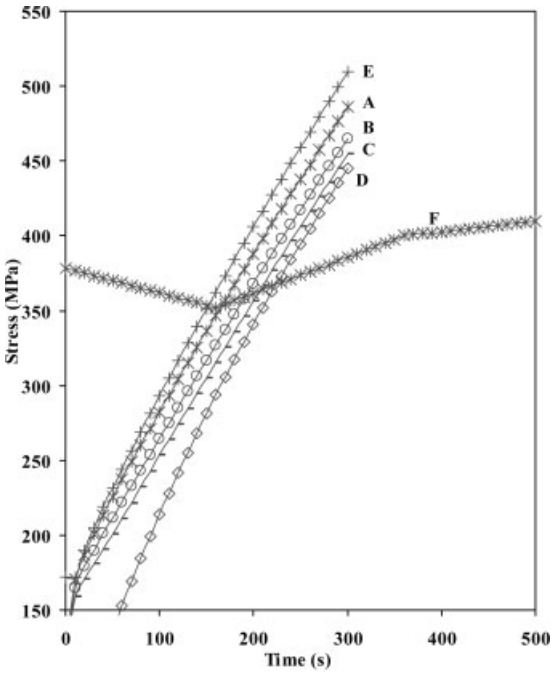

Figure 9. Comparison of UTS against total tangential stresses in the pipe wall during fire attack.

Curve A: 25 mm; curve B: 50 mm; curve C: 75 mm; curve D: 100 mm; curve E: isolated pipeline; curve F: UTS.

The governing theory for predicting the fluid dynamics within the pipeline and that of the escaping fluid is based on the numerical solution of the conservation equations using the MOC in conjunction with a suitable equation of state. The earlier coupled with the simulated triaxial thermal and pressure stresses within the pipeline wall form the basis for a comprehensive model for producing a timeline presentation of the failure mechanism of pressurized pipelines during fire attack.

Using a hypothetical example involving a pressurized natural gas pipeline, two types of failure scenarios were quantitatively analyzed. The first involved direct jet fire impingement on the isolated pipeline.

Examination of the resulting triaxial stress data revealed that during thermal loading, the prevailing tangential compressive thermal stresses in the inner pipe wall rapidly transform into much larger tensile forces toward the outer wall. Once these stresses exceed the pipe wall material yield stress, the pipeline begins to deform by bulging.

With the passage of time, further rise in the temperature of the pipe wall results in an increase in the tensile stress at the outer wall. The pipeline catastrophically fails through rupture when this stress exceeds the vessel wall material UTS.

Emergency depressurization is found to have a significant impact on delaying the time to failure with the effect increasing with increasing relief valve diameter. Much the same as that for the isolated pipeline, the prevailing failure mode is found to be due to tangential tensile stresses at the outer pipe wall surface.

Finally, the model presented in this article can be used as an extremely useful tool for comprehensive safety assessment of pressurized pipelines during fire attack. It will, for the first time, enable operators of pressurized pipelines to predict how relief valve size influences the time-to-failure for jet fire impingement with high heat fluxes and possibly circumvent failure at lower heat flux exposures.

Literature Cited

1. Bond J. IChemE accidents database, IChemE, Rugby, U.K., 2002.
2. Pipeline and Hazardous Materials Safety Administration (PHMSA), Office of Pipeline Safety. http://ops.dot.gov.
3. HInt Dossier, Hazards intelligence, Näsilinnankatu 30-B32, 33200 Tampere, Finland, 2005:32–38.
4. Pipeline safety instrument for the control of major accident hazards involving pipelines, Joint Research Centre, European Commission, Major Accident Hazards Bureau, Ispra (Va), Italy, 1999.
5. Regulatory benchmark for the control of major accident hazards involving pipelines, European Commission Draft Directive on Pipeline Safety, Major Accident Hazards Bureau, Brussels, 2004.
6. Beynon GV, Cowley LT, Small LM, Williams I. Fire engulfment of LPG tanks: HEATUP, a predictive model. *J Hazard Mater*. 1988;20: 227–238.
7. Ramskill PK. A description of the "ENGULF" computer codes—to model the thermal response of an LPG tank either fully or partially engulfed by fire. *J Hazard Mater*. 1988;20:177–196.
8. Mahgerefteh H, Falope GBO. Modelling transient stresses in spherical vessels during blowdown under fire attack. *AIChE J*. 2003;49: 1307–1316.
9. Ozisik MN. *Heat Conduction*. New York: Wiley, 1980.
10. Holman JP. *Heat Transfer*. New York: McGraw Hill, 1986.
11. Fire and explosion guidance, Part 2: Avoidance and mitigation of fires, UKOOA/HSE, London, 2006 (final draft).
12. Gnielinski V. New equations for heat and mass transfer in turbulent pipe and channel flows. *Int Chem Eng*. 1976;16:359–367.
13. Steiner D, Taborek J. Flow boiling heat transfer in vertical tubes correlated by an asymptotic method. *Heat Transfer Eng*. 1992;13: 43–69.
14. Mahgerefteh H, Saha P, Economou IG. Fast numerical simulation for full bore rupture of pressurized pipelines. *AIChE J*. 1999;45: 1191–1201.
15. Mahgerefteh H, Saha P, Economou IG. Modelling fluid phase transition effects on dynamic behaviour of ESDV. *AIChE J*. 2000;46: 997–1006.
16. Mahgerefteh H, Oke A, Rykov Y. Efficient numerical simulation for highly transient flows. *Chem Eng Sci*. 2006;61:5049–5056.
17. Mahgerefteh H, Oke A, Atti O. Modelling outflow following rupture in pipeline networks. *Chem Eng Sci*. 2006;61:1811–1818.
18. Mahgerefteh H, Atti O, Denton G. An interpolation technique for rapid CFD simulation of highly transient flows. *Trans Inst Chem Eng Part B: Process Safety Environ Protect*. 2006;84:45–50.
19. Zucrow MJ, Hoffman JD. *Gas Dynamics*, Vols. I and II. New York: Wiley, 1976:297.
20. Oke A, Mahgerefteh H, Economou I, Rykov Y. A transient outflow model for pipeline puncture. *Chem Eng Sci*. 2003;58:4591–4604.
21. Chen JR, Richardson SM, Saville G. Modelling of two-phase blowdown from pipelines. I. A hyperbolic model based on variational principles. *Chem Eng Sci*. 1995;50:695–713.
22. Chen JR, Richardson SM, Saville G. Modelling of two-phase blowdown from pipelines. II. A simplified numerical method for multicomponent mixtures. *Chem Eng Sci*. 1995;50:2173–2187.
23. Haque MA, Richardson SM, Saville G. Blowdown of pressure vessels. I. Computer model. *Trans Inst Chem Eng Part B: Process Safety Environ Protect*. 1992;70:5–11.
24. Mahgerefteh H, Wong SMA. A numerical blowdown simulation incorporating cubic equations of state. *Comput Chem Eng*. 1999;23: 1309–1317.
25. Massey BS. *Mechanics of Fluids*. Wokingham, U.K.: Van Nostrand Reinhold, 1983.
26. Peng DY, Robinson DB. A new two-constant equation of state. *Ind Eng Chem Fund*. 1976;15:59–64.

27. Millat J, Dymond JH, Nieto de Castro CA, editors. *Transport Properties of Fluids: Their Correlation, Prediction and Estimation*. IUPAC. Cambridge: Cambridge University Press, 1996.
28. Assael MJ, Martin Trusler JP, Tsolakis T. *Thermophysical Properties of Fluids*. London: Imperial College Press, 1996.
29. Michelsen ML. The isothermal flash problem. I. Stability. *Fluid Phase Equilib*. 1982;9:1–19.
30. Michelsen ML. The isothermal flash problem. II. Phase-split calculation. *Fluid Phase Equilib*. 1982;9:21–40.
31. Michelsen ML. Multi-phase isenthalpic and isentropic flash algorithms. *Fluid Phase Equilib*. 1987;33:13–27.
32. Picard DJ, Bishnoi PR. Calculation of the thermodynamic sound velocity in two-phase multi-component fluids. *Int J Multiphase Flow*. 1987;13:295–308.
33. Popov EP. *Engineering Mechanics of Solids*. Englewood Cliffs, NJ: Prentice Hall, 1999.
34. Timoshenko SP, Goodier JN. *Theory of Elasticity*. New York: McGraw-Hill, 1987.
35. Brandes EA, editor. *Smithells Metals Reference Book*. London: Butterworths, 1983.

Manuscript received Nov. 29, 2006, and revision received Jun 29, 2007.